Ambient single particle analysis in Riverside, California by aerosol time-of-flight mass spectrometry during the SCOS97-NARSTO

ARTICLE *in* ATMOSPHERIC ENVIRONMENT · JANUARY 2003

Impact Factor: 3.28 · DOI: 10.1016/S1352-2310(03)00393-5

PERGAMON

AE International – North America

Atmospheric Environment 37 Supplement No. 2 (2003) S239–S258

ATMOSPHERIC ENVIRONMENT

www.elsevier.com/locate/atmosenv

Ambient single particle analysis in Riverside, California by aerosol time-of-flight mass spectrometry during the SCOS97-NARSTO

Sylvia H. Pastor[a], Jonathan O. Allen[b,1], Lara S. Hughes[b], Prakash Bhave[b], Glen R. Cass[†], Kimberly A. Prather[c,*]

[a] *Department of Chemistry, University of California, Riverside, CA 92521-0403, USA*
[b] *Environmental Engineering Science Department, MC 138-78, California Institute of Technology, Pasadena, CA 91125, USA*
[c] *Department of Chemistry and Biochemistry, University of California, 9500 Gilman Drive, La Jolla, CA 92093-0314, USA*

Received 8 February 2002; accepted 31 March 2003

Abstract

Single-particle measurements were made using aerosol time-of-flight mass spectrometry (ATOFMS) instruments in conjunction with the 1997 Southern California Ozone Study-North American Research Strategy for Tropospheric Ozone (SCOS97-NARSTO). The size and chemical composition of individual ambient particles in Riverside, CA during the summer of 1997 are described. Data collected using co-located micro-orifice uniform deposit impactors (MOUDI) impactors are used to scale the ATOFMS number counts, providing a unique picture of the particle population which complements information obtained using traditional sizing and composition analysis techniques in this and previous studies. Changes in single particle composition are observed over time, and compared and contrasted with observed changes in visibility, ozone, and PM_{10} concentrations. Details are provided on changes in the particle size and composition observed during three morning periods with low ozone and elevated PM_{10} versus three afternoon periods with both elevated ozone and PM_{10} levels between 21–23 August 1997. The ATOFMS size profiles show afternoon periods dominated by sub-μm particles composed of organic carbon coupled with ammonium nitrate, and morning periods with relatively high levels of super-μm dust particles. The observed changes in particle size and composition are consistent with differences in air mass trajectories arriving at Riverside during the morning and afternoon time periods.

Temporal variations in single particle types detected over a 40 day sampling period are presented, demonstrating the type of unique information that can be obtained regarding atmospheric particle processes through long term sampling studies. The broader availability of single particle mass spectrometers coupled with recent advances in the field are now providing unique information on the associations of multiple chemical species (i.e. mixing state) within individual particles with high size and temporal resolution.

Keywords: Aerosol; Chemistry; On-line; Particulate matter; Neural network

1. Introduction

Human health, mortality, and global climate change issues regarding ambient particles are well documented (Charlson et al., 1987; Dockery et al., 1993; Vedal, 1997; Pope, 2000; Dockery, 2001; Penner et al., 2001). The Los Angeles area is notorious for generating and accumulating high levels of airborne pollutants due to

*Corresponding author. Tel.: +1-858-822-5312; fax: +1-858-534-7042.
E-mail address: kprather@ucsd.edu (K.A. Prather).
[1] Present address: College of Engineering and Applied Sciences, Arizona State University, Tempe, AZ 85287-6006, USA.
[†] Deceased.

1352-2310/03/$ - see front matter © 2003 Elsevier Ltd. All rights reserved.
doi:10.1016/S1352-2310(03)00393-5

the combined effects of gas and particle phase emissions primarily from vehicles along with intense sunlight, mountain-surrounded geography, and atmospheric conditions, including light winds and the common occurrence of an inversion layer (Lawson, 1990; Dolislager and Motellebi, 1999). To further our understanding of aerosols in the southern California region, intensive atmospheric measurements of particle and gas phase species were made during the 1997 Southern California Ozone Study-North American Research Strategy for Tropospheric Ozone (SCOS97-NARSTO) field campaign that took place in southern California during the summer and fall of 1997. The Southern California Air Quality Study (SCAQS), conducted 10 years prior to this study, was the only other field study conducted in southern California of this magnitude (Lawson, 1990). Many of the findings from SCOS97-NARSTO are consistent with those from SCAQS (Chow et al., 1994; Gao et al., 1994; Turpin and Huntzicker, 1995; Eldering and Cass, 1996), although new results emerged due in part to new technology developments for aerosol analysis that have occured over the past decade (McMurry, 2000). During SCAQS, using mainly bulk analysis techniques, the most abundant species and the largest components of $PM_{2.5}$ were identified as nitrate, sulfate, ammonium, organic carbon, and elemental carbon (Chow et al., 1994). In contrast, species such as sodium, aluminum, silicon, calcium, and iron were abundant in the PM_{10} fraction. However, the combinations of chemical species present on individual particles could not be identified during SCAQS. Information on the chemical associations as a function of particle size is vital to understanding the sources of the particles, subsequent chemistry the particles undergo in the atmosphere, as well as the health effects of particles (Thomas and Morawska, 2002).

This paper focuses on real-time single particle mass spectrometry measurements made with an aerosol time-of-flight mass spectrometry (ATOFMS) instrument in Riverside, an area situated on the eastern edge of the Los Angeles air basin and characterized by extended periods of high smog levels and poor air quality. ATOFMS was one of the first real-time single particle mass spectrometry (SPMS) techniques to be used in field campaigns. A number of recent reviews describe the various SPMS instruments (Suess and Prather, 1999; Johnston, 2000). Murphy et al. (1998) have performed extensive ambient sampling using PALMS in other areas (Murphy and Thomson, 2000), however until recently, the majority of single particle measurements have focused on relatively simplistic, laboratory generated particles (Neubauer et al., 1998; Kane and Johnston, 2001; Phares et al., 2001; Kane et al., 2002). Subtle yet fundamental differences in each of the instruments general operating principles lead to differences in the information they provide, particularly on size-resolved chemistry (Middlebrook et al., 2003). The ability to size particles in PALMS is limited by the light scattering method used for particle detection (Lee et al., 2002). Other SPMS instruments select a specific particle size and must step through multiple discrete sizes, limiting the size resolution and increasing the time required to fully interrogate a statistically representative number of atmospheric particles (Mallina et al., 2000; Held et al., 2002). SPMS instruments have the potential to provide unique insights into atmospheric aerosols, however currently a bottleneck associated with processing the extensive ambient data sets exists. A number of efforts are underway to develop routine procedures which can be used to extract information from the data in formats that allow for rapid comparison with other particle, gas phase, and meteorological measurements (Hinz et al., 1999; Phares et al., 2001; Bhave et al., 2002a; Held et al., 2002; Tan et al., 2002). This paper focuses on some of the methodologies used in our laboratory as well as the unique insights single particle data can provide once the data are reduced to the appropriate format.

Three aerosol time-of-flight mass spectrometers analyzed particulate matter in different locations in the Los Angeles Basin. From June until October 1997, the lab-based ATOFMS instrument sampled in Riverside. In addition to the ATOFMS instruments, electrical aerosol analyzers and laser optical particle counters measured particle size distributions. During intensive sampling periods, fine particle ($<1.9\,\mu m$) and PM_{10} filter samplers were used to obtain bulk chemical composition data. Particles in several size ranges were measured using a pair of micro-orifice uniform deposit impactors (MOUDIs) at each site for selected times during the intensive sampling periods in order to scale the ATOFMS data using a procedure described previously (Allen et al., 2000).

This paper describes the sized-resolved composition observed for particles with aerodynamic diameters between 0.2 and 1.6 μm sampled in Riverside. The ATOFMS provides unique information on the combinations of chemical species present in individual particles as a function of particle size, such as the couplings between sulfates and nitrates with specific particle types in the different size modes. In general, the strength of single particle mass spectrometers lies in the ability to obtain individual particle fingerprints for performing source identification and apportionment, as well as monitoring secondary transformations on particles. The ultimate goal is to use the chemical associations observed in single particle data for model comparisons (Kleeman et al., 1997; Kleeman and Cass, 2001; Bhave et al., 2002b), as well as to provide input into atmospheric aerosol models (Pandis et al., 1992; Jacobson, 1999).

The individual particle chemical data in Riverside were acquired with high temporal resolution to allow

direct (hour by hour) comparisons to be made between the particle types observed with gas phase (i.e. ozone), meteorology, and visibility data. Data collected over a 3-day period between 21 and 23 August 1997 are discussed, comparing and contrasting the aerosol size and composition distributions observed during periods with elevated ozone and PM_{10} levels. In addition, long term trends observed over a 40-day period in Riverside of several particle types are discussed, showing the advantages to real-time measurements of particle composition with high temporal resolution over extended periods of time.

2. Experimental details

Aerosol time-of-flight mass spectrometry is described in a number of previous publications (Prather et al., 1994; Gard et al., 1997). ATOFMS provides continuous, real-time detection and characterization of single particles from polydisperse samples, supplying information on particle size and composition. The lab-based ATOFMS instrument sampled air from a second floor window of the Chemistry building on the University of California-Riverside campus continuously from 29 June to 30 September 1997. ATOFMS instruments pull air into a sample inlet region. A converging nozzle followed by a region of differential pumping with skimmers creates a narrow particle beam. Each particle is accelerated to a size-dependent terminal velocity. Particles in the collimated beam scatter light as they cross continuous-wave diode laser beams. The velocity of each particle is determined from the transit time between two continuous-wave laser beams located a known distance apart. The aerodynamic diameter is calculated from a calibration curve relating the velocity of the particle to an aerodynamic diameter. The firing of a pulsed laser—a frequency quadrupled Nd:YAG (266 nm, Continuum)—is triggered based on the velocity of the particle to desorb/ionize species from the particle. The ions generated from the ablation process are analyzed by time-of-flight mass spectrometry. The lab-based instrument used for this study in Riverside is capable of detecting positive or negative ion mass spectra. During this study in Riverside, about 30 min of every 3 h were dedicated to negative ion data collection. Positive and negative ion mass spectra provide complementary information on the chemical species present in the particles. Since the positive and negative ion mass spectra are not directly comparable, only the periods where positive ion spectra were acquired are discussed in this paper. A break appears in the temporal plots for each 30-min period when negative ion mass spectra were being acquired.

The single-particle ATOFMS data are calibrated for size using a calibration curve that is generated by measuring the velocity of ammonium sulfate $(NH_4)_2(SO_4)$ particles generated with a vibrating orifice aerosol generator (VOAG; TSI, Inc.) and polystyrene latex spheres (PSL) of known aerodynamic diameters. The size calibration was performed in the range $0.2\,\mu m < D_a < 2.5\,\mu m$. The mass spectra are calibrated using custom written software. Peak lists are generated for each mass spectrum collected. A peak threshold of 10 units above baseline and an area threshold of 12 units were used for creating the peak lists.

The detection efficiency calibration functions for the Southern California Ozone Study were derived in an analogous manner to those developed by Allen and coworkers for a study that took place in southern California in 1996 (Allen et al., 2000). The particle detection efficiency is a function of particle aerodynamic diameter (D_a). For the lab-based instrument, the calibration equation was determined to be $N = 1500(D_a)^{-4.2}$. Note this represents the average for the entire study obtained by using all calibration points. Further details on how this equation changed over the course of the study are given in Bhave et al. (2002a). Applying a single calibration equation to the entire study simplified the overall calibration procedure, but in future studies, different calibrations corresponding to specific periods of the study will be used. For a given volume of air, the number of particles present in the ambient air sample, N, may be calculated using the size of each particle observed by ATOFMS. The application of the scaling factors to a size distribution has a larger effect on smaller-sized particles, due to their smaller detection efficiency. The ATOFMS inlet used during the present study focused a narrow size range of particles very efficiently, leading to enhanced particle detection in the 1.6–1.8 μm size range. Because this size interval is much narrower than the corresponding size range of MOUDI measurements used to calibrate these data (1.0–1.8 μm), the MOUDI calibration could not account for the ATOFMS focusing effect, so the ATOFMS data above 1.6 μm are disregarded in the present work. In future studies, calibration will be attempted using aerosol instruments that sample at finer size resolutions than the MOUDI, such as aerodynamic particle sizers.

The neural network selected for mass spectral classification is an adaptive resonance algorithm, known as ART-2a (Carpenter et al., 1991). ART-2a identifies classes of particles, and has previously been applied to sets of single-particle data, including ATOFMS data (Hopke and Song, 1997; Song et al., 1999; Phares et al., 2001). Matlab (Mathworks Inc.) is used for the ART-2a analysis. A database, YAADA, manages and allows for the analysis of single-particle ATOFMS data (Allen, 2001). The data are imported into YAADA, an object-oriented toolbox written in the Matlab programming language (Matlab versions 5.3 and 6.0 were used for this analysis). Pentium-based PC computers running

Windows 98 are used for the data processing. Each particle to be analyzed by ART-2a is converted into a normalized vector where each point represents a whole mass-to-charge unit in the mass spectrum. ART-2a clusters particles that have sufficiently similar vectors. Each class or cluster of particles has an associated weight vector which describes the "quintessential" mass spectrum for that class. Clusters determined by the neural network are compared and classes with similar chemical composition, size, and temporal profiles may be combined. The set of weight vectors is called a weight matrix. The parameters for the ART-2a analysis included: a vigilance factor of 0.5, a learning rate of 0.05, a maximum of 20 iterations, and a range of the first 350 mass-to-charge (m/z) units of the positive ion mass spectra for creating the vectors.

Because this data set was so large, special analysis procedures were developed in order to allow the computer to process the data. An initial subset of particles was analyzed to determine the major particle types. The initial analysis set contained 11,480 particles from eight 1-h time periods starting with the following times: 21 August 1997 at 1:00, 12:00, 21:00; 22 August 1997 at 6:00, 15:00, 24:00; and 23 August 1997 at 9:00, 18:00. This initial data set created a matrix of weight vectors, one for each class of particles. Then each particle in this 3-day ATOFMS data set was classified into these types. All particles that could not be classified by the existing types were analyzed by a second ART-2a analysis, generating additional classes in the form of a second weight matrix. Finally, the combined set of classes from both ART-2a analyses was used to classify the entire set of particles a final time. In summary, four general steps were taken to arrive at the final particle classes from the ART-2a analysis: ART-2a analysis of the initial data set, matching the full set to those classes, ART-2a analysis of unclassified particles with the generation of additional classes, and matching the full set to the combined set of classes.

The South Coast Air Quality Management District (SCAQMD) provided the ozone and PM_{10} hourly data. Electric Power Research Institute (EPRI) provided the hourly nephelometer data. The b_{scat} data provide a measure of the light reduction due to the scattering of light by gases and particles present in the ambient sample. Electric Power Research Institute (EPRI) and Harvard University-School of Public Health (HSPH) provided daily $PM_{2.5}$ mass data. These measurements were all made at the University of California Agricultural Operations Field about a mile from the ATOFMS sampling site.

Air parcel trajectory plots created by backward integration through hourly wind fields were calculated from the wind speed and direction observations from about 30 sites in the air basin. In this study, the trajectories of air parcels arriving hourly at Riverside on 21–23 August 1997, were calculated using the method of Goodin et al. (1979).

3. Results and discussion

3.1. ART-2a analysis of ATOFMS data (21–23 August 1997)

The Riverside ATOFMS collected 90,585 positive-ion mass spectra of individual particles from 21 to 23 August 1997. Positive-ion time-of-flight mass spectra were obtained for approximately 30 percent of the sized particles. Using ART-2a, all of the particles from the three-day period were classified into 57 clusters based on their similarity to the weight vectors. These clusters were sorted and assigned numbers based on the number of spectra explained by each cluster. Seventy percent of the analyzed particles were accounted for by the top 10 clusters, 86 percent by the top 20, 95 percent by the top 30, and 98 percent by the top 40 clusters. Less than half of a percent of the particles, 488 out of 90,585, did not match any of the 57 weight vectors within the vigilance factor (VF = 0.5).

A summary of cluster information for the 20 most populated clusters, based on unscaled ATOFMS counts, is given in Table 1. In the table, the clusters are sorted from the most to the least populated based on unscaled ATOFMS counts. ATOFMS instruments preferentially detect larger particles so the rank order of the types changes for detection-efficiency scaled ATOFMS data. The 12 most intense ion peaks are listed for each cluster. To provide an indication of the relative intensity of the peaks within each weight vector, the mass-to-charge ratios (m/z) are presented in coded typeface as described in the caption. The characteristic chemical markers in each of the 20 dominant clusters are briefly assigned in the far right column of Table 1. The particle mass spectra show markers for amines, ammonium nitrate, calcium, iron, organic carbon (OC), elemental carbon (EC), sea salt, and other particle types. The top 20 clusters will be discussed in further detail, including their chemical composition, size, and temporal profiles.

3.2. Chemical composition of particle classes determined by ART-2a analysis

The "quintessential" mass spectra of the top 20 clusters from the ART-2a analysis are shown in Figs. 1–3, in the form of normalized intensity versus mass-to-charge (m/z). These weight vectors represent the mass spectra when normalized and reduced to unit mass resolution. Although masses up to 350 m/z were considered in the ART-2a analysis, the range plotted for each weight vector is truncated to highlight the range with the most characteristic peaks, the first 100 m/z units

Table 1
Summary of particle classes identified by ART-2a

Class #	No. in class	Top 12 peaks (m/z)[a]												Brief description
1	24,234	**23**	39	24	40	63	41	46	36	62	108	25	30	Sea salt
2	15,488	23	24	**39**	40	25	63	41	26	62	108	165	46	Sea salt, nitrate, sulfate
3	5061	40	23	**41**	24	57	39	56	59	42	44	25	26	Calcium, sodium-rich dust
4	3034	**27**	**37**	**18**	**43**	**36**	**12**	**30**	39	29	24	86	38	Organic carbon, amines
5	2997	**39**	**40**	**41**	23	57	56	27	24	140	72	42	64	Potassium-rich dust
6	2891	**40**	**57**	**56**	41	27	39	113	23	24	42	96	44	Calcium-rich dust
7	2861	**39**	23	41	56	24	1	40	27	43	18	42	36	Potassium-rich dust
8	2509	**30**	**18**	12	35	36	27	31	46	17	37	24	43	Nitrate, ammonium, carbon
9	2338	39	**27**	**23**	40	56	41	24	28	57	1	25	26	Potassium-rich dust
10	1783	1	**23**	**24**	**27**	39	16	25	26	40	38	28	22	Soil dust
11	1718	37	**36**	**27**	43	18	38	39	12	86	50	24	30	Organic carbon, amines
12	1701	18	**37**	**43**	**30**	**27**	39	36	12	38	29	24	51	Ammonium, carbon, nitrate
13	1654	30	18	**12**	27	43	37	36	24	39	29	17	28	Nitrate, ammonium, carbon
14	1623	**51**	**67**	27	37	18	43	36	39	23	30	12	38	Vanadium-rich, carbon
15	1561	**56**	39	57	40	27	23	54	2	1	51	41	24	Iron-rich dust
16	1493	**36**	**12**	37	24	27	43	18	30	39	48	23	60	Elemental carbon
17	1493	12	**36**	**24**	27	37	18	30	43	29	39	28	17	Elemental carbon
18	1424	2	**16**	**23**	**27**	39	25	24	26	28	40	29	41	Soil dust
19	1264	2	24	**27**	28	17	40	16	29	39	26	25	41	Soil dust
20	1229	2	**25**	**17**	**28**	23	27	40	24	29	26	41	16	Soil dust

[a] Normalized area: >**0.75**; 0.5−0.75; **0.25**−**0.50**; <0.25

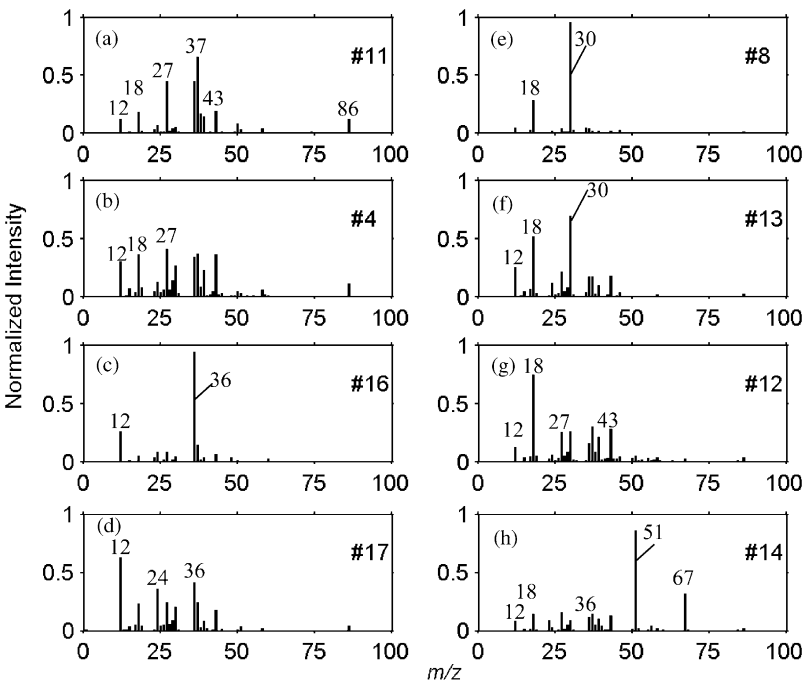

Fig. 1. Normalized weight vectors for common organic particle classes identified by ART-2a: (a) cluster 11 organic carbon with amines I, (b) cluster 4 organic carbon with amines II, (c) cluster 16 elemental carbon I, (d) cluster 17 elemental carbon II, (e) cluster 8 ammonium nitrate I, (f) cluster 13 ammonium nitrate II, (g) cluster 12 ammonium nitrate III, and (h) cluster 14 vanadium-rich.

of the positive ion mass spectra. The chemical composition of the particles may be inferred from the weight vectors.

The normalized weight vectors for eight clusters that have characteristic organic carbon marker peaks are presented in Fig. 1. Clusters 4, 8, 11, 12, 13, 14, 16, and

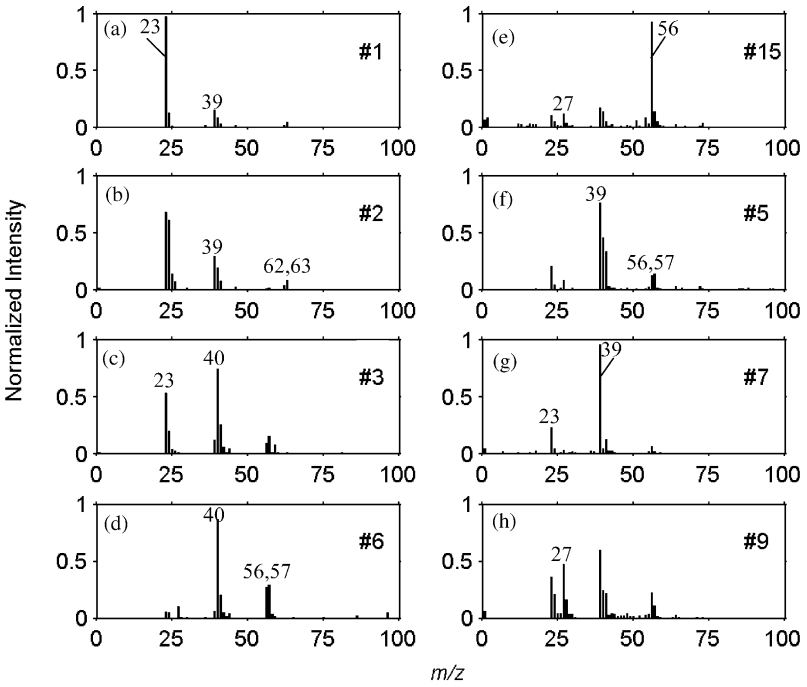

Fig. 2. Normalized weight vectors for common inorganic particle classes identified by ART-2a: (a) cluster 1 sea salt I, (b) cluster 2 sea salt II, (c) cluster 3 calcium-rich I, (d) cluster 6 calcium-rich II, (e) cluster 15 iron-rich, (f) cluster 5 potassium-rich I, (g) cluster 7 potassium-rich II, and (h) cluster 9 potassium-rich III.

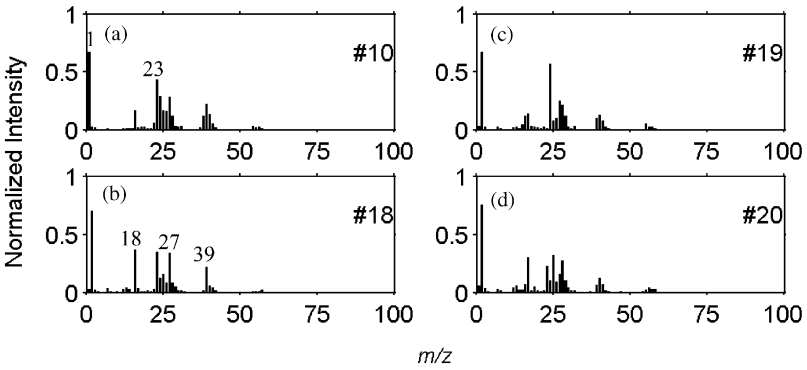

Fig. 3. Normalized weight vectors for common soil dust particle classes identified by ART-2a: (a) cluster 10, (b) cluster 18, (c) cluster 19, and (d) cluster 20.

17 show organic and elemental carbon fragment peaks at m/z 12(C^+), 27($C_2H_3^+$/CHN^+), 36(C_3^+), 37(C_3H^+), and 43(CH_3CO^+/$CHNO^+$). There are other possible assignments for many of the peaks but the most likely assignments are given in parentheses. Combustion processes, such as vehicle exhaust, are a major source of carbon particles in this area. In addition, these particles, while moving through the basin to Riverside, can accumulate organic carbon species from a variety of sources (Hughes et al., 2000). The weight vectors for clusters 4 and 11 have a peak at m/z 86. Based on smog chamber experiments, the most likely assignment for this peak is $^{86}[(C_2H_5)_2\ N{=}CH_2]^+$, a commonly observed fragment of alkylamines which partition to the particles in an analogous manner to gas phase ammonia reacting with nitric acid (Angelino et al., 2001). Clusters 16 and 17 possess distinct elemental carbon signatures, and are most likely derived from vehicles (Watson et al., 1994). Carbon peaks, including $^{12}C^+$, $^{24}C_2^+$, and $^{36}C_3^+$ are among the most intense for these elemental carbon

clusters, consistent with the findings of Kawamura et al. (2000) in Los Angeles. Clusters 16 and 17 are considered together as elemental carbon based on their similar composition and size and temporal profiles. Peaks at m/z 18 and 30 appear in the carbon particle weight vectors, showing the accumulation of ammonium and nitrate ($^{18}(NH_4)^+$ and $^{30}(NO)^+$) on carbon particles as they are transported into Riverside. These species represent secondary coatings of sub-μm carbon particles with ammonium nitrate, generated by the gas-to-particle reaction between ammonia and nitric acid (Russell and Cass, 1986; Wall et al., 1988; Hughes et al., 2002). Particles in cluster 12 also show a strong ammonium nitrate signature blended with organic carbon. Ammonium nitrate-enriched particles are well documented in a number of studies in southern California (Wall et al., 1988; Chow et al., 1994), as well as previous ATOFMS studies in Riverside (Liu et al., 2000). Finally, the weight vector for cluster 14 contains OC peaks similar to clusters 4 and 11, as well as vanadium and vanadium oxide peaks, $^{51}V^+$ and $^{67}(VO)^+$ (Fig. 1h). These species are produced by fuel oil combustion (Lyyranen et al., 1999; Suarez and Ondov, 2002).

Clusters 1, 2, 3, 5, 6, 7, 9, and 15 show a variety of distinct inorganic signatures (Fig. 2). The particles in clusters 1 and 2 are sea-salt particles. Sea-salt type particles are commonly detected in Riverside, located about 60 miles east of the Pacific coast (Song et al., 1999). The mass spectral markers for sea salt include $^{23}Na^+$, $^{39/41}K^+$, $^{40}Ca^+$, $^{62}(Na_2O)^+$, $^{108}(Na_2NO_3)^+$ and $^{165}(Na_3SO_4)^+$. While the weight vectors of clusters 1 and 2 have several features in common, they were distinguished as unique classes by ART-2a due to the fact that peaks at m/z 108 and 165 are more prominent for particles in cluster 2. These peaks indicate these particles had undergone reactions with gas phase NO_x and SO_x species while being transported inland (Pilinis et al., 1987; Chow et al., 1994; Gard et al., 1998; Kerminen et al., 1998; Roth and Okada, 1998). Calcium marker peaks at $^{40}Ca^+$ and $^{57}(CaOH)^+$ are among the most intense peaks for clusters 3 and 6. A high number of Ca-containing particles were observed in previous studies in nearby Rubidoux (Chow et al., 1992, 1994; Kim et al., 2000a, b). Despite the similarity in chemical signatures, the temporal trends of calcium-rich clusters 3 and 6 are different, thus supporting the assignment by ART-2a as two unique calcium-rich classes. This represents a good example of where obtaining dual ion spectra would offer an advantage, as the negative ion spectrum would most likely be different and provide a better indication of the potential source of these particles (Gard et al., 1997). Cluster 15 contains typical soil dust peaks, including $^{23}Na^+$, $^{27}Al^+$, and $^{39}K^+$, $^{56}Fe^+$, and $^{40}Ca^+$ and $^{57}(CaOH)^+$ (Silva et al., 2000). Fe-rich particles have also been observed by Chow et al. in Rubidoux. The particles in clusters 5, 7, and 9 have $^{39}K^+$ as the most intense peak. Since the composition, size, and temporal profiles for clusters 5 and 7 are similar, they are grouped together as one class. These clusters may represent particles of the same origin/source with spectra that differ slightly due to shot-to-shot variability in laser powers rather than being truly different particle types. However, cluster 9 has a different temporal profile, particularly on 21 August, and thus was not grouped with clusters 5 and 7.

Fig. 3 shows the normalized weight vectors of four other inorganic particle clusters: 10, 18, 19, and 20. These weight vectors often have peaks at 23, 27, 39, and 40 and have an intense peak at m/z 1–2. The peaks in these spectra are wide with non-Gaussian shapes, which resulted in miscalibrated peaks for clusters 18, 19, and 20. Because they have similar size and temporal profiles with the peaks just shifted by one m/z unit, the particles in clusters 10, 18, 19, and 20 are merged together and labeled as soil dust. Inland locations, such as Rubidoux, near Riverside, have aerosols enriched in nitrate and soil dust (Solomon et al., 1989).

It should be noted, that in general, ammonium and nitrate marker ions were observed in sub-μm particle spectra much more commonly than super-μm particles during this study. Almost 100% of the organic carbon particle spectra in clusters 4, 8, 12, and 13 show peaks indicative of ammonium (m/z 18) and nitrate (m/z 30). Between 60% and 80% of the particle spectra for clusters 11, 14, and 17 show peaks due to ammonium and nitrate. In contrast, 40–60% of the particles in the sea-salt clusters (1, 2) contained markers due to nitrate and only 4–11% due to ammonium (m/z 18). As indicated, the nitrate peak at m/z 30 in these particles is due to heterogeneous reaction between sea-salt particles and gaseous NO_x species. For the inorganic particle types, 11–18% and 4–5% of the particles in clusters 3 and 6 (Ca-rich) contained markers for nitrate and ammonium, respectively. In the other dust clusters (5, 7, 9, 10, 15, 18–20), between 20–50% and 5–20% contained markers due to nitrate and ammonium, respectively. Note that a higher fraction of dust particles contained markers for nitrate than ammonium. This most likely indicates the nitrate peaks are a product of heterogeneous reactions of NO_x with the dust particles and not gas-to-particle conversion of ammonium nitrate (Grassian, 2002). It should be noted that the upper end of the percentages were typically observed during the afternoon periods, during stagnant conditions. This difference in partitioning between fine and coarse particles is consistent with previous studies which predict a difference in partitioning for particles of different sizes due to the time scales required for the particles to achieve equilibrium, with smaller particles achieving equilibrium with gas phase species much faster than larger particles (Meng and Seinfeld, 1996).

3.3. Size distributions of particle classes determined by ART-2a

Figs. 4 and 5 show the size profiles of organic and inorganic clusters, respectively, plotted with 0.1 μm resolution. In these plots, the histograms are not scaled for instrumental transmission/detection efficiency, since relative difference between the times periods are more apparent with uncorrected ATOFMS data. Examples of scaled ATOFMS data are shown in Fig. 10. The different particle types detected by the instrument tend to be centered either above or below 1 μm. This well-defined break is consistent with previous studies conducted in southern California (Noble and Prather, 1996; Hughes et al., 1999, 2000; Song et al., 1999; Raes et al., 2000), as well as other locations (Guazzotti et al., 2001; Kegler et al., 2001; Thomas and Morawska, 2002; Wilson et al., 2002).

The size histograms for the common organic clusters show a large number of the particles have aerodynamic diameters of less than 1 μm (Fig. 4). The size profile for cluster 8 is uniquely bimodal (Fig. 4e). The super-μm particles in cluster 8 appear in a narrow time range on 23 August, peaking at about 10:00, as noted previously by Liu et al. in a paper describing nitrate-containing particles in Riverside, CA (Liu et al., 2000). The particles in cluster 12 are mostly super-μm and occur during the late afternoon of 21 August (Fig. 4g). In this case, from the single particle data, the coarse mode ammonium is associated with nitrate in OC particles and not with wind-blown soil, a possible scenario suggested by John et al. (1990) in a previous study. The vanadium-rich particles are sub-μm, as observed in other studies in southern California as well as other countries (Cahill et al., 1996; Singh et al., 2002; Thomas and Morawska, 2002). The size histograms of the common inorganic clusters are super-μm, and most likely the lower size end of mechanically-generated (coarse) particles (Fig. 5). Inorganic clusters 5, 7, and 15 show bimodal size distributions, indicating ART-2a at a vigilance factor of 0.5 combined K-rich and Fe-rich particles produced by combustion sources (sub-micron) with inorganic dust/soil coarse (super-micron) particle types. In summary, the size profiles show particles of organic carbon, elemental carbon, and ammonium nitrate types primarily in the sub-μm range. In contrast, the sea salt, inorganic-enriched dusts, and soil dust particle types occur primarily in the super-μm range. These size profiles suggest that a $PM_{1.0}$ standard could generally distinguish combustion generated particles (EC, OC) from sea salt and dust in the Riverside aerosol, as the composition changes significantly around 1 μm, a finding that is consistent with a number of other previous studies.

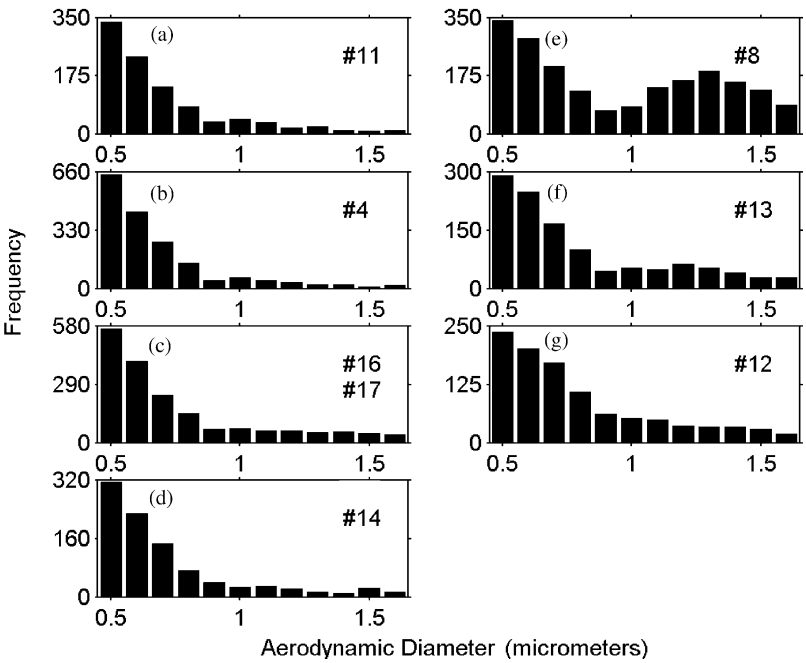

Fig. 4. Size distribution plots for common organic particle classes identified by ART-2a: (a) cluster 11 organic carbon with amines I, (b) cluster 4 organic carbon with amines II, (c) grouped clusters 16 and 17 elemental carbon, (d) cluster 14 vanadium-rich (e) cluster 8 ammonium nitrate I, (f) cluster 13 ammonium nitrate II, and (g) cluster 12 ammonium nitrate III.

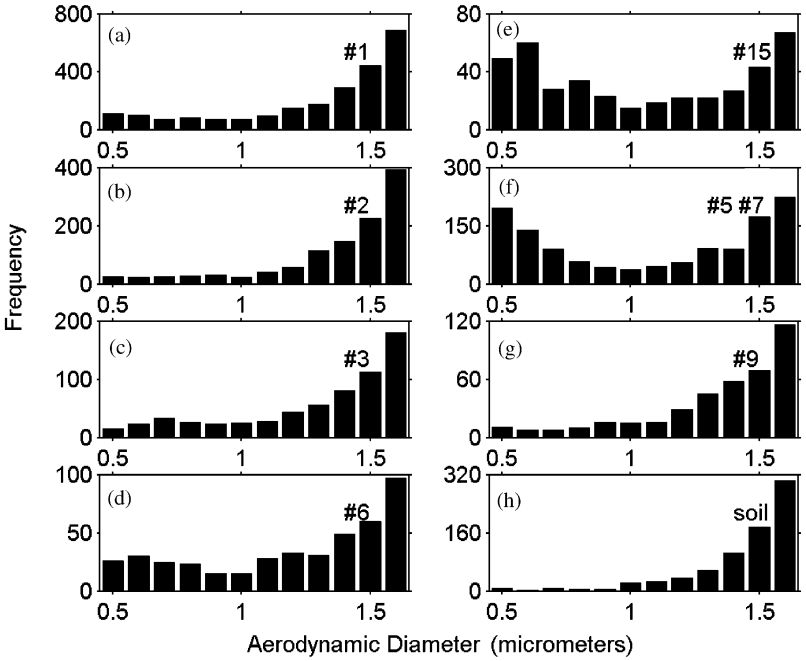

Fig. 5. Size distribution plots for common inorganic particle classes identified by ART-2a: (a) cluster 1 sea salt I, (b) cluster 2 sea salt II, (c) cluster 3 calcium-rich I, (d) cluster 6 calcium-rich II, (e) cluster 15 iron-rich, (f) grouped clusters 5 and 7 potassium-rich, (g) cluster 9 potassium-rich III, and (h) grouped clusters 10, 18, 19, and 20 soil dust.

3.4. Temporal characteristics of Riverside air quality

Hourly ozone, PM_{10}, and b_{scat} data are shown in Fig. 6. Hourly $PM_{2.5}$ data were not available for Riverside during this period. Four daily $PM_{2.5}$ measurements were available, 23.5 h averages starting at 10:00. The average values for 21, 22, and 23 August were 13, 28, and 24 $\mu g\,m^{-3}$, respectively. The trajectory plots for six time periods are shown in Fig. 7. The temporal profiles of the most common ATOFMS particle classes are shown in Figs. 8 and 9.

Hourly average ozone values in Riverside on 21–23, August 1997 peaked each afternoon (Fig. 7). Each morning, the hourly PM_{10} level peaked and a second, smaller PM_{10} peak occurred each afternoon. The afternoon peak in the b_{scat} and PM_{10} data coincided with the daily ozone peak. The PM_{10} values rose each morning while the ozone levels remained low. The b_{scat} values show a peak each morning, a larger peak each afternoon, and an additional peak at 1:00 on 23 August. It is interesting to note that the b_{scat} peak on the morning of 22 August was the smallest peak in the 3-day period yet the PM_{10} levels were at their highest. The ATOFMS data can be used to help explain this observation by identifying the types of particles present during these periods.

Based on the ambient data, six time periods of interest were chosen. The three afternoon periods of high ozone levels occurred on 21 August 14:00–16:00, 22 August 17:00, and 23 August 13:00, during which the b_{scat} values also increased. The three time periods with low ozone levels and high PM_{10} levels occurred on 21 August 7:00, 22 August 8:00, and 23 August 8:00. The average morning ozone level was only 10 ppb, but the afternoon average was over 100 ppb. The average morning b_{scat} was 0.14×10^{-4} m^{-1} and the afternoon average was 0.20×10^{-4} m^{-1}. The average morning PM_{10} peak was about 100 $\mu g\ m^{-3}$ and the afternoon average was 70 $\mu g\ m^{-3}$.

Trajectory plots shown in Fig. 7 indicate the paths of the air masses arriving in Riverside. The open circles represent the location of the air parcel at consecutive hours for 60 h before the air mass reached Riverside. Overlapping circles indicate stagnation of the air parcel, which usually occurred overnight between about 20:00 and 10:00 and sometimes for longer periods of time. On 21 August, air parcels had come from over the Pacific and east of Catalina Island. On 22 and 23 August, the trajectory plots show the air masses arriving from over the Pacific, north of Catalina Island. Some air masses stagnated near the Mira Loma area that has dairies and elevated levels of gas phase ammonia (Russell et al., 1988; Solomon et al., 1988). The trend from 21–23 August showed that air masses spent progressively more and more time over land. It can be immediately noted that the 23 August air masses spent the most time over

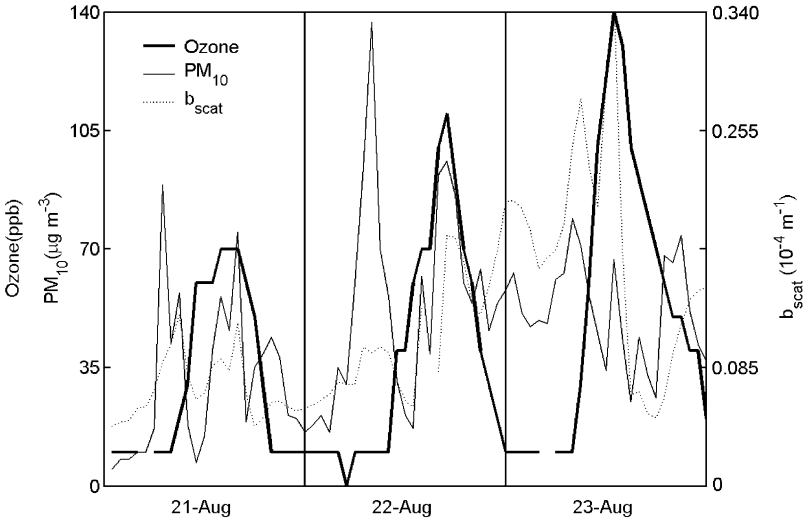

Fig. 6. Time series plots for hourly ozone, PM_{10}, and b_{scat} measurements for Riverside.

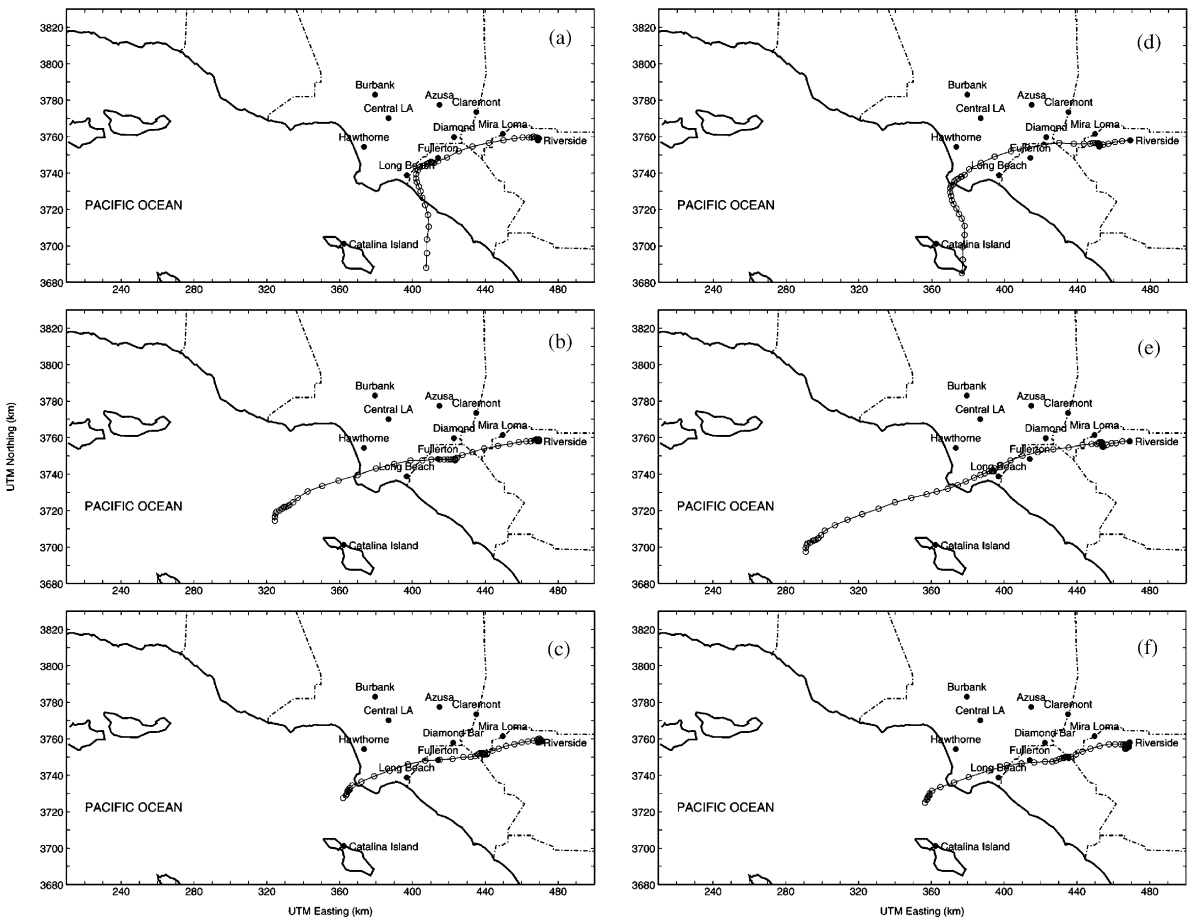

Fig. 7. Representative air parcel trajectories arriving in Riverside, CA during elevated PM_{10} periods at: (a) 7:00 21 August 1997, (b) 8:00 22 August 1997, (c) 8:00 23 August 1997, and elevated ozone at: (d) 16:00 21 August 1997 (e) 17:00 22 August 1997(f) 13:00 23 August 1997.

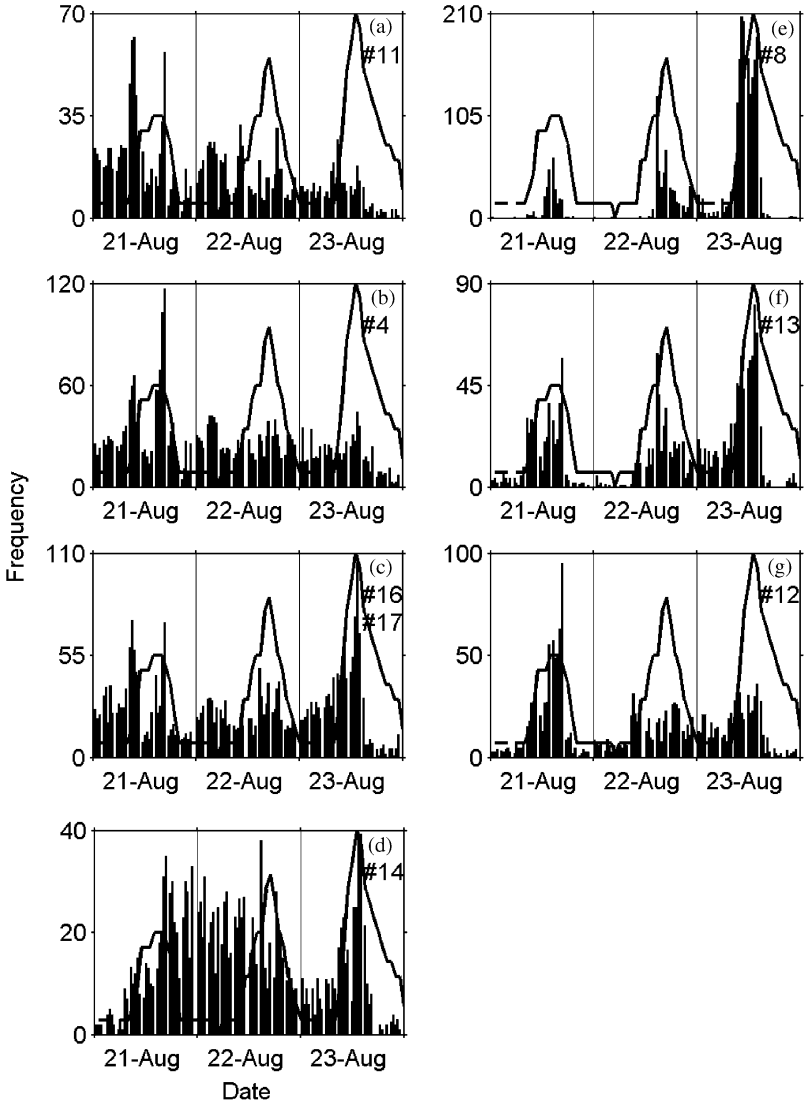

Fig. 8. Time series plots of common organic particle classes identified by ART-2a: (a) cluster 11 organic carbon with amines I, (b) cluster 4 organic carbon with amines II, (c) grouped clusters 16 and 17 elemental carbon, (d) cluster 14 vanadium-rich, (e) cluster 8 ammonium nitrate I, (f) cluster 13 ammonium nitrate II, and (g) cluster 12 ammonium nitrate III with the temporal trend ozone overlaid. Temporal resolution is 30 min for the single-particle data and 60 min for the ozone data.

land because almost all of the 60 data points shown on 23 August occur over land. The air masses spending more and more time over land is consistent with the increasing daily ozone peak concentrations observed 21–23 August as well as an increased presence of pollution-derived particles.

The ATOFMS size profiles of the particles in Riverside obtained during the times of interest generally show two modes with a break at 1 μm. It is important to note that during the afternoon, elevated-ozone time periods show a larger contribution from particles in the sub-μm mode relative to those in the super-μm mode. This is consistent with the optical particle counter and particle filter data. The optical particle counter data show an increase in the sub-μm particle mass concentration in the afternoons, particularly between 0.5 and 1 μm, accompanied by a decrease in the super-μm particle mass concentration. Also the fine ($<1.9\,\mu m$) and coarse ($<10\,\mu m$) particle filter samples, collected by the Cass research group on 21 and 22 August in Riverside, show slightly higher morning coarse particle concentrations and a doubling of the fine particle concentration between the morning and afternoon on 21 August. The particle size distribution

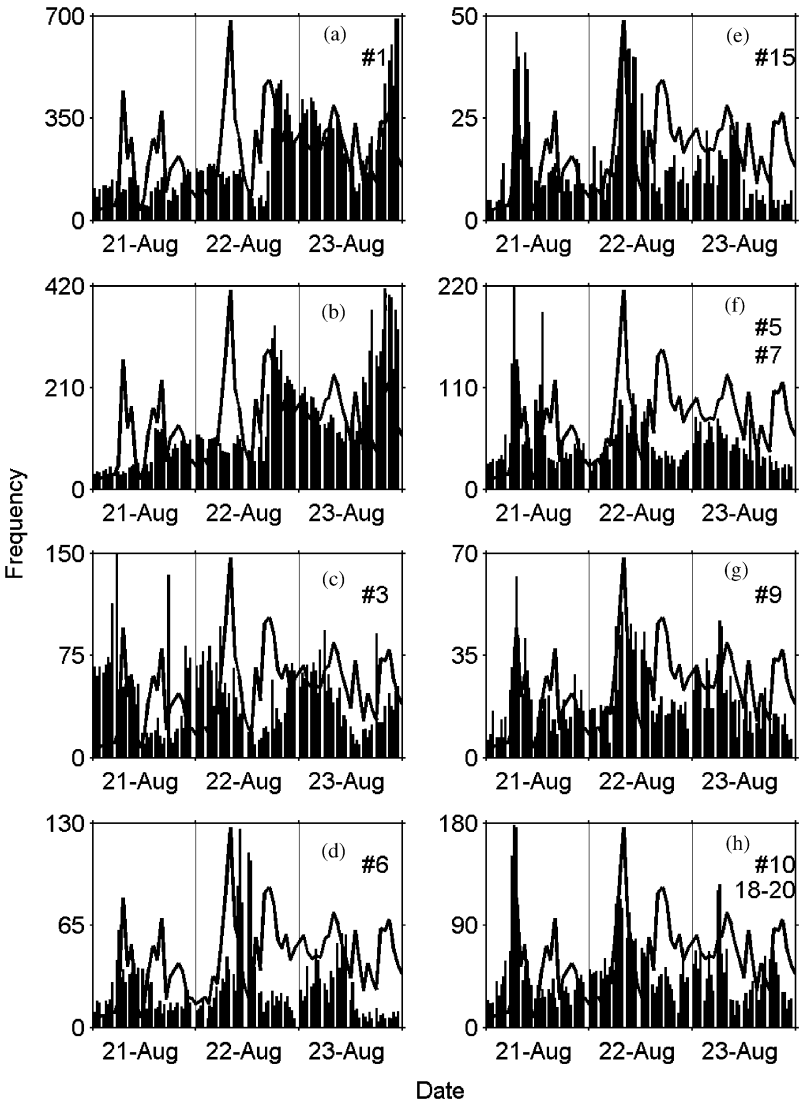

Fig. 9. Time series plots for common inorganic particle classes identified by ART-2a: (a) cluster 1 sea salt I, (b) cluster 2 sea salt II, (c) cluster 3 calcium-rich I, (d) cluster 6 calcium-rich II, (e) cluster 15 iron-rich, (f) grouped clusters 5 and 7 potassium-rich, (g) cluster 9 potassium-rich III, and (h) grouped clusters 10, 18, 19, and 20 soil dust with the temporal trend of PM_{10} overlaid. Temporal resolution is 30 min for the single-particle data and 60 min for the PM_{10} data.

clearly shifts between the morning and afternoon periods. The ATOFMS data show simultaneous particle composition changes that further explain the changes in visibility.

The temporal plots of the various particle-composition types in Figs. 8 and 9 (with 30 min resolution) show when each of the particle types was detected. If the ATOFMS instrument collected positive ion mass spectra for less than 24 of the 30 min (i.e. offline for greater than 20% of the time), no data are plotted. For all remaining time periods, the ATOFMS data were scaled upward to estimate the actual number of particles that would have been acquired in a full half-hour period to account for the small amount of offline time in any given period. Fig. 8 shows the temporal histograms for the organic clusters: 4, 8, 11, 12, 13, 14, and 16/17. Fig. 9 shows the temporal histograms for the inorganic clusters: 1, 2, 3, 6, 9, 15, 5/7, and 10/18/19/20. The temporal trends of the PM_{10} or ozone are plotted with each cluster's temporal profile. It is important to note the afternoon PM_{10} and b_{scat} peaks generally coincide with the ozone peak. In examining these plots, it is possible to see the particle types that correlate with the ozone levels versus the PM_{10} levels.

Of the various particle types, cluster 13 tracks the temporal profile for ozone (Fig. 8f), with cluster 8 having the next closest correlation (Fig. 8e). A larger sub-μm mode of ammonium-nitrate-organic carbon particles appears during the periods of elevated ozone in the afternoon. These midday peaks in fine particle nitrate are consistent with data from previous field campaigns in southern California (John et al., 1990; Wexler and Seinfeld, 1992). Clusters 8 and 13 particles occur only when the ozone levels are high. Furthermore, it is important to note that these particle types disappear immediately when the marine layer arrives in Riverside, particularly on the afternoon of 23 August which is evident upon comparison of Figs. 8e and f with Figs. 9a and b, respectively. It is interesting to note that the visibility levels increase dramatically when the marine layer arrives and clusters 8 and 13 disappear, however the ozone levels decrease much more slowly. This is the first time such a clear cut correlation between specific particle types (clusters 8 and 13) and gas phase species (ozone) has been observed with ATOFMS. A possible explanation for the observed gas and particle phase correlations could be that typical ambient air in Riverside is composed of an excess of gas phase ammonia, and thus the formation of ammonium nitrate is limited by the availability of nitric acid. This is consistent with other studies in the Riverside area, including one performed later in 1997 (Lurmann et al., 1997; Hughes et al., 2002). In this case, the ozone concentrations could be serving as a surrogate measure of the ambient nitric acid levels, with increases in ozone corresponding to increased nitric acid levels, leading to an increase in the numbers of particles containing significant amounts of ammonium nitrate (clusters 8 and 13).

The wind trajectories for the afternoon periods on 21 and 22 August show the air parcels stagnated over land near Mira Loma before reaching Riverside (Fig. 7d–e), and thus the arriving air masses had a significant dairy-influence from stagnation. The trajectory for the air mass arriving during the largest ozone peak in the 3-day period, on 23 August, stagnated over Riverside for about 18 h (Fig. 7f). The rapid appearance of the ammonium-nitrate-organic carbon particles coupled with the stagnant nature of the air masses indicate that the associated chemical processes are occurring in Riverside and not being transported in from another location. During the extended stagnation episode on 23 August, the particles grew through condensation and agglomeration processes giving a unique size distribution with a small peak above the sub-μm particles. The ATOFMS results indicate the ammonium-nitrate-organic carbon particles are responsible for the decreased visibility in Riverside during this time period. In fact, looking closely at the b_{scat} profile, one notices a peak in the b_{scat} just before the ozone peak, corresponding to an increase in the ammonium-nitrate-organic carbon particles. Furthermore, as previously described, when these particles disappear upon arrival of the marine front, the b_{scat} values immediately decrease as well. The close tracking of this particle type with visibility may add to our understanding of the specific particle types that have the strongest influence on atmospheric visibility (Watson, 2002).

The temporal profiles of some of the inorganic clusters while not peaking with ozone do track the morning PM_{10} concentrations (Fig. 9). The particles in the sea-salt classes peak just after the ozone level maxima on all 3 days (Fig. 9a,b), marking the arrival of cleaner air masses. The wind trajectories show that sea salt enriched air masses arriving in Riverside, such as 22 August 1997 20:00 (not shown) stagnated at the coast before making landfall, explaining the dominance of sea-salt particles. Following the stagnation period at the coast, the estimated time over land for this sea-salt enriched air mass was relatively short, leaving little time for the particles to become transformed by land-based emissions. The fresh marine air mass replaced the polluted afternoon air mass that has stagnated for so many hours in Riverside.

One of the calcium-rich particle types, cluster 3, shows a strong diurnal variation, peaking each morning around 3:00. Its presence is generally anti-correlated with ozone (Fig. 9c). A local source of these calcium-rich particles or possibly the transport downward from higher altitudes would be among the most logical explanations for this type of particle because the wind trajectories show no significant movement during these time periods. With substantial calcium-related ion signals, cluster 6 is similar to cluster 3, however the particles in cluster 3 contain more sodium. The temporal profiles of these clusters are different, indicating different sources (Fig. 9c,d). The soil and metal-rich dust particles peak in number during the morning PM_{10} peaks (Fig. 9e–h). The temporal profile of cluster 6 is similar to the temporal profile of soil dust suggesting the cluster 6 particles may be of crustal/soil origin (Fig. 9d,h). A daytime peak in potassium-rich particles has also been observed in Central California (Chow et al., 1999). Inorganic particle types make larger contributions to the super-μm mode observed during the morning periods when elevated PM_{10} levels occur.

3.5. Scaled size distributions with particle composition

The ATOFMS mass spectral and particle size data provide a summary of the size-composition relationships of the individual particle types as shown in Fig. 10. The particles were grouped into broader particle types based on the class descriptions in Table 1 to generate the composition information within the bars of size histograms. Classes 1 and 2 are labeled sea salt; classes 3 and 6 are calcium-rich; classes 4 and 11 are organic carbon

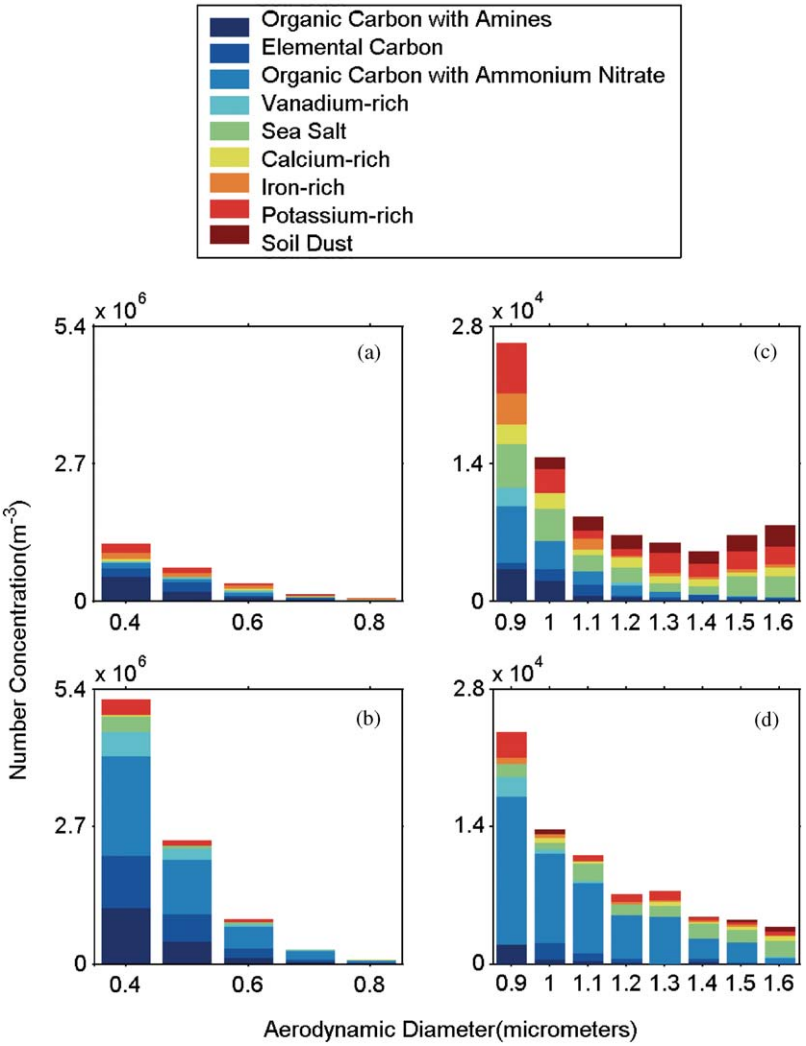

Fig. 10. Scaled size distribution plots for Riverside, CA during time periods with elevated PM_{10} (a) and (c) and elevated ozone (b) and (d). These plots represent an average of 6:30–7:30 21 August, 7:30–8:30 22 August, and 7:30–8:30 23 August 1997, in (a) and (c) and of 14:30–15:30 21 August, 16:30–17:30 22 August and 12:30–13:30 23 August 1997. Each bar is color coded for the general chemical composition.

with amines; classes 5, 7, and 9 are potassium-rich; classes 8, 12, and 13 are organic carbon with ammonium nitrate; class 10, 18, 19, and 20 are soil dust; class 16 and 17 are elemental carbon; class 14 is vanadium-rich, and class 15 is iron-rich. The particles in these classes account for over 85 percent of the total particles and 80 percent or more of the particles in each time period plotted. The remainder of the particles in the less common classes (clusters 21–57) are omitted from Fig. 10 to simplify the plot.

The size distributions for the morning periods with elevated PM_{10} and low ozone levels, 10a and 10c (upper), are represented by the average of the ATOFMS data from 21 August at 7:00, 22 August at 8:00, and 23 August at 8:00. The afternoon periods, 10b and 10d (lower), with elevated levels of ozone, PM_{10}, and b_{scat}, are represented by an average of the ATOFMS data from 21 August at 15:00, 22 August at 17:00, and 23 August at 13:00. The plot for each time period has been separated into two size ranges to allow the presentation of data over a large concentration range. The scaled number concentrations for 0.4–0.9 μm particles appear in Fig. 10a,b, while the scaled number concentration information for 0.9–2.5 μm particles appears in Fig. 10c,d. The *y*-axes are shown with the same range for the two time periods to allow for direct comparison of the relative change in the number concentration data. The representative number concentrations were gener-

ated from the ATOFMS data using the detection-efficiency calibration function which was calculated by comparison of seven pairs of ambient Riverside aerosol ATOFMS and MOUDI data sampled during SCOS97-NARSTO (Bhave et al., 2002a) (Fig. 10).

Each day was unique, but similar general trends are apparent. The trends are consistent in both the unscaled and scaled ATOFMS data. The individual particle types present in Riverside are dramatically different between the morning and afternoon periods. The morning periods were characterized by the presence of sea-salt, metal-rich-dust, and soil-dust particles in the super-μm mode. In contrast, the afternoon ozone episodes were characterized by sub-μm particles composed of organic carbon, elemental carbon, ammonium, nitrate, and amines. Based on the single particle mass spectra and the MOUDI measurements used to calibrate the ATOFMS data, dust accounts for a significant fraction of the particulate matter mass in Riverside, including when the highest PM_{10} level of almost $140\,\mu g\,m^{-3}$ was reached in Riverside (see Fig. 9). Based on the ATOFMS data, in addition to contributing to PM_{10} mass, sea-salt and dust particles can make contributions to $PM_{2.5}$. This is consistent with observations of soil in the $PM_{2.5}$ fraction in Phoenix (Kegler et al., 2001). Based on this observation, we also conclude that the current $PM_{2.5}$ regulation would not allow one to distinguish between combustion derived and inorganic particle sources. Particulate matter episodes and most of the pollution burden in southern California are attributed to the many industries and vehicles present. In this study, other sources are shown to make significant contributions to the $PM_{2.5}$ mass concentrations under certain meteorological conditions.

3.6. Scaled size distributions with particle composition

As described, during SCOS97-NARSTO, the ATOFMS collected a nearly continuous data set in Riverside between 19 August 1997 and 27 September 1997. The cost associated with high size and temporal resolution analysis size-resolved composition data for this long has historically prohibited one from obtaining. SPMS instruments can now be used to obtain such information. Examining an extended data set reflects whether short term trends in particle composition as described above are unique to a limited 3-day period or whether they are typical (Pitchford and Green, 1997). Over the 40-day sampling period, 1,141,941 positive ion spectra were acquired. Several of the particle types showed consistent diurnal patterns of varying magnitudes. In Fig. 11, the time series plot for cluster 6, the super-μm, calcium-rich dust type is shown. The temporal profile of cluster 6 particles shows a regular pattern of morning peaks with similar intensity for all 40 days. It is important to note that these data represent unscaled ATOFMS counts. However the relative trends (maxima and minima) are accurate; scaling would only change the absolute number concentrations. These trends can be explained by the typical local wind patterns in Riverside where the air stagnates overnight beginning around 20:00 and begins to undergo movement around 10:00,

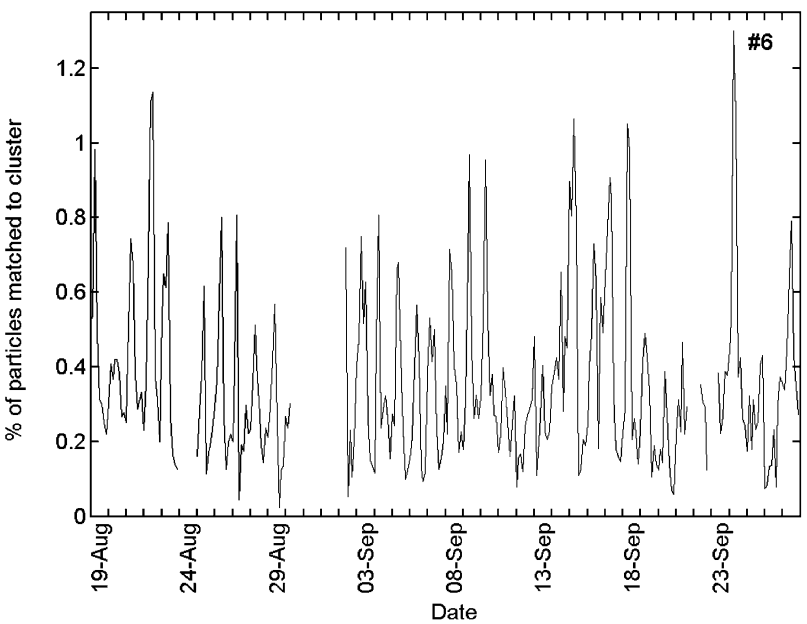

Fig. 11. Time series plot for particles matched to calcium-rich dust cluster 6. Temporal resolution is 3 h for the single-particle data.

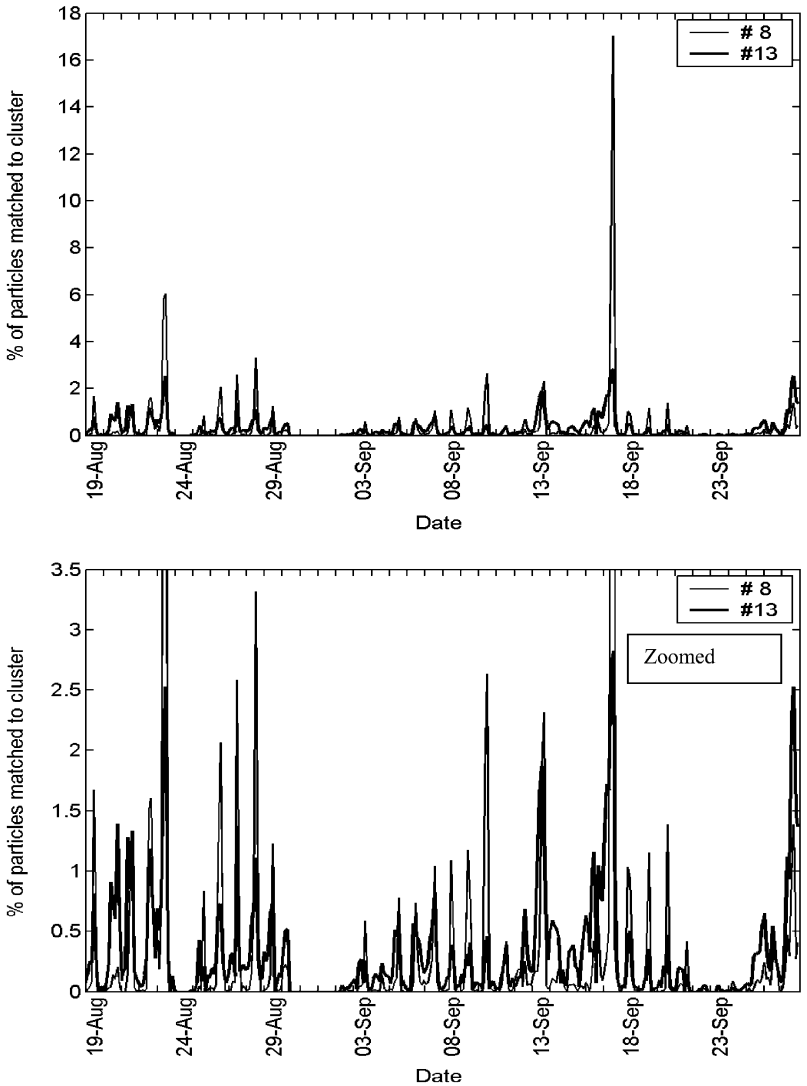

Fig. 12. Time series plots for particles matched to organic carbon with ammonium nitrate clusters 8 and 13. Temporal resolution is 3 h for the single-particle data. The lower plot has a "zoomed-in" y-axis.

diluting this particle type. Residence times for air flow in southern California are typically on the order of 12 h during the summer periods (Meng and Seinfeld, 1996).

As mentioned in Section 3.4, the afternoon episodes of 21–23 August were characterized by the increased presence of sub-μm-sized, carbon-rich particles, especially ammonium-nitrate-organic carbon particles that correlated with increased ozone levels. The ammonium-nitrate-organic-carbon clusters 8 and 13 particles show interesting temporal trends for 21–23 August 1997 (see Fig. 8e,f) and now with the larger data set may be examined over the 40 day period with 3 hour resolution. In Fig. 12, the two ammonium-nitrate-organic carbon classes (8 and 13) are shown with similar temporal trends, consistent with the 21–23 August period. Other days also exhibit peaks, indicating the appearance of organic carbon ammonium nitrate particles. The greatest number of cluster 8 particles in a single 3-h period occurred on 17 September 1997 (17% of the total particles detected matched cluster 8 during this time period). These particles show a normal, bimodal unscaled ATOFMS size distribution, with the large mode dominating the unscaled particle size distribution. The particles in clusters 8 and 13 were not randomly distributed throughout the day but instead displayed a diurnal pattern with maxima occurring between 12:00 and 15:00. The peak for cluster 8 particles is somewhat more narrow and intense. The peaks at m/z 18 and 30

have a greater relative intensity for cluster 8 than for cluster 13. It appears that cluster 8 particles are only present at the heart of an ammonium nitrate episode. Cluster 13 particles appear to represent more of a general indicator of an ammonium nitrate episode, appearing slightly before and after the cluster 8 particles. It is possible these particle types are the same with just different thicknesses of ammonium and nitrate. Coupling the real-time ATOFMS data acquisition with real-time particle classification would provide a means for recognizing certain episodes. This information could be used, for example, to choose when to sample with filter-based techniques in order to obtain further information on the chemical nature of the particles during such episodes.

The 40 days of data are useful for determining the commonality of the peaks in particle composition. For example, particles in cluster 8 peak on 13 and 17 September appear as isolated spikes in the temporal profile while peaks on 21–23, 25–28 August and 5–8 September appear as sets of days with increasing peak frequency values. Having this broader perspective on the air quality with high resolution, allows one to determine the significance of an event or particle type in a certain location. Data at this level of detail can be used to test predictions from air quality models to obtain a better understanding of atmospheric aerosol processes.

4. Conclusions

This paper provides details on the individual particle types present during 21–23 August 1997 as well as 40 days of continuous sampling in Riverside, CA, showing the temporal variations of common particle types. The particles were classified by ART-2a analysis, creating 57 classes. The major particle types in Riverside, CA included organic carbon with amines, elemental carbon, organic carbon, ammonium nitrate, sea salt, soil dust, and various metal-rich types. A comparison of the particle types present during morning peaks of high PM_{10} and low ozone is made with afternoon periods with high ozone, PM_{10}, and b_{scat}. The combination of ATOFMS to determine particle size and composition, and neural networks to classify those particles creates a powerful method for describing the ambient particle population and distinguishing differences in the particle population.

On 21–23 August 1997, two types of air pollution episodes, mornings with elevated PM_{10} and afternoons with elevated ozone, were shown to have different size distributions and were characterized by particles of different chemical composition. Inorganic particle types, super-μm dust with some sea-salt particles, characterized the morning episodes. Soil and other dust-type particles were particularly evident during the morning episodes on 21 and 22 August. The afternoon episodes were characterized by the increased presence of sub-μm carbon-rich particles, especially ammonium-nitrate-organic carbon particles which correlated with increased ozone levels. Sea salt and ammonium nitrate-organic particle types were anti-correlated throughout the study. The b_{scat} values tended to track the organic-ammonium nitrate particle types, particularly during the afternoon ozone events. Air parcel trajectories linked particle types to the air mass paths across the Los Angeles Basin, including a link between ammonium nitrate enriched organic carbon particle and stagnation near dairies in Mira Loma.

Contradicting theories exist as to whether coarse ($>2.5\,\mu m$) or fine ($<2.5\,\mu m$) particles produce health effects (Brunekreef and Holgate, 2002). This is partly because during certain times, one size range of particles has been shown to produce a certain effect, while at other times this same size range of particles has shown no effect. These conflicting results are most likely due to the fact that at different times and locations, the size cut at $PM_{2.5}$ does not separate compositions from different sources (i.e. coarse particles (i.e. dust, sea salt) from accumulation mode particles (i.e. combustion (organic)), and therefore cannot separate the effects due to fine and coarse particulate matter. Particles from such different sources have been shown to have quite different health effects (Laden et al., 2000; Morawska and Zhang, 2002). This study confirms $PM_{1.0}$ would be more effective at separating particles from these sources which produce drastically different compositions. This same size-composition trend has been shown previously in other ATOFMS studies conducted in other regions of the United States and world including the Indian Ocean (Guazzotti et al., 2001), Atlanta (Liu et al., 2003; Wenzel et al., 2003), Texas, as well as bulk source combustion studies and ambient size distribution measurements (Kleeman et al., 1999; Morawska and Zhang, 2002; Salma et al., 2002). Based on these findings, in future health effects studies, using a cut-point at 1 μm (as opposed to 2.5 μm) would most likely provide results which are less ambiguous and easier to interpret from day to day and location to location.

Acknowledgements

The authors express thanks to the Prather Group members (past and present) who assisted with ATOFMS data acquisition during SCOS97-NARSTO. The authors are grateful to David Fergenson for assistance with Matlab and YAADA. The authors express thanks to the SCAQMD for the ozone and PM_{10} data, thanks to EPRI (Alan Hanson) for the b_{scat} data, and thanks to EPRI and the Harvard School of Public Health (George Allen and Petros Koutrakis) for the daily $PM_{2.5}$ mass

data. This research was supported by California Air Resources Board (#96-307) and the US Environmental Protection Agency (STAR Fellowship U-91556601).

References

Allen, J.O., 2001. YAADA: software toolkit to analyze single-particle mass spectral data. Software reference manual.

Allen, J.O., Fergenson, D.P., Gard, E.E., Hughes, L.S., Morrical, B.D., Kleeman, M.J., Gross, D.S., Gaelli, M.E., Prather, K.A., Cass, G.R., 2000. Particle detection efficiencies of aerosol time of flight mass spectrometers under ambient sampling conditions. Environmental Science and Technology 34, 211–217.

Angelino, S., Suess, D.T., Prather, K.A., 2001. Formation of aerosol particles from reactions of secondary and tertiary alkylamines: characterization by aerosol time-of-flight mass spectrometry. Environmental Science and Technology 35, 3130–3138.

Bhave, P.V., Allen, J.O., Morrical, B.D., Fergenson, D.P., Cass, G.R., Prather, K.A., 2002a. A field-based approach for determining ATOFMS instrument sensitivities to ammonium and nitrate. Environmental Science and Technology 36, 4868–4879.

Bhave, P.V., Kleeman, M.J., Allen, J.O., Hughes, L.S., 2002b. Evaluation of an air quality model for the size and composition of source-oriented particle classes. Environmental Science and Technology 36, 2154–2163.

Brunekreef, B., Holgate, S.T., 2002. Air pollution and health. Lancet 360, 1233–1242.

Cahill, T.A., Morales, R., Miranda, J., 1996. Comparative aerosol studies of Pacific Rim cities—Santiago, Chile (1987); Mexico City, Mexico (1987–1990); and Los Angeles, U.S.A. (1973 and 1987). Atmospheric Environment 30, 747–749.

Carpenter, G.A., Grossberg, S., Rosen, D.B., 1991. Art 2a—an adaptive resonance algorithm for rapid category learning and recognition. Neural Networks 4, 493–504.

Charlson, R.J., Lovelock, J.E., Andreae, M.O., Warren, S.G., 1987. Oceanic phytoplankton, atmospheric sulfur, cloud albedo and climate. Nature (London, UK) 326, 655–661.

Chow, J.C., Liu, C.S., Cassmassi, J., Watson, J.G., Lu, Z., Pritchett, L.C., 1992. A neighborhood-scale study of PM10 source contributions in Rubidoux, California. Atmospheric Environment 26A, 693–706.

Chow, J.C., Watson, J.G., Fujita, E.M., Lu, Z., Lawson, D.R., Ashbaugh, L.L., 1994. Temporal and spatial variations of PM2.5 and PM10 aerosol in the Southern California air quality study. Atmospheric Environment 28, 2061–2080.

Chow, J.C., Watson, J.G., Lowenthal, D.H., Hackney, R., Magliano, K., Lehrman, D., Smith, T., 1999. Temporal variations of PM2.5, PM10, and gaseous precursors during the 1995 integrated monitoring study in central California. Journal of the Air and Waste Management Association 49, PM/16–PM/24.

Dockery, D.W., 2001. Epidemiologic evidence of cardiovascular effects of particulate air pollution. Environmental Health Perspectives 109, 483–486.

Dockery, D.W., Pope III, C.A., Xu, X., Spengler, J.D., Ware, J.H., Fay, M.E., Ferris, B.G., Speizer, F.E., 1993. An association between air pollution and mortality in six US cities. New England Journal of Medicine 329, 1753–1759.

Dolislager, L.J., Motellebi, N., 1999. Characterization of particulate matter in California. Journal of the Air and Waste Management Association 49 PM-45–PM-56.

Eldering, A., Cass, G.R., 1996. Source-oriented model for pollutant effects on visibility. Journal of Geophysical Research 101, 19343–19369.

Gao, N., Cheng, M.-D., Hopke, P.K., 1994. Receptor modeling of airborne ionic species collected in SCAQS. Atmospheric Environment 18, 1447–1470.

Gard, E., Mayer, J.E., Morrical, B.D., Dienes, T., Fergenson, D.P., Prather, K.A., 1997. Real-time analysis of individual atmospheric aerosol particles: design and performance of a portable ATOFMS. Analytical Chemistry 69, 4083–4091.

Gard, E.E., Kleeman, M.J., Gross, D.S., Hughes, L.S., Allen, J.O., Morrical, B.D., Fergenson, D.P., Dienes, T., Galli, M.E., Johnson, R.J., Cass, G.R., Prather, K.A., 1998. Direct observation of heterogeneous chemistry in the atmosphere. Science (Washington, DC) 279, 1184–1187.

Goodin, W.R., McRae, G.J., Seinfeld, J.H., 1979. A comparison of interpolated methods for sparse data: application to wind and concentration fields. Journal of Applied Meteorology 18, 761–771.

Grassian, V.H., 2002. Chemical reactions of nitrogen oxides on the surface of oxide, carbonate, soot, and mineral dust particles: implications for the chemical balance of the troposphere. Journal of Physical Chemistry A 106, 860–877.

Guazzotti, S.A., Coffee, K.R., Prather, K.A., 2001. Continuous measurements of size-resolved particle chemistry during INDOEX-intensive field phase 99. Journal of Geophysical Research-Atmospheres 106, 28607–28627.

Held, A., Hinz, K.P., Trimborn, A., Spengler, B., Klemm, O., 2002. Chemical classes of atmospheric aerosol particles at a rural site in central Europe during winter. Journal of Aerosol Science 33, 581–594.

Hinz, K.P., Greweling, M., Drews, F., Spengler, B., 1999. Data processing in on-line laser mass spectrometry of inorganic, organic, or biological airborne particles. Journal of the American Society for Mass Spectrometry 10, 648–660.

Hopke, P.K., Song, X.H., 1997. Classification of single particles by neural networks based on the computer-controlled scanning electron microscopy data. Analytica Chimica Acta 348, 375–388.

Hughes, L.S., Allen, J.O., Kleeman, M.J., Johnson, R.J., Cass, G.R., Gross, D.S., Gard, E.E., Gaelli, M.E., Morrical, B.D., Fergenson, D.P., Dienes, T., Noble, C.A., Liu, D.-Y., Silva, P.J., Prather, K.A., 1999. Size and composition distribution of atmospheric particles in southern California. Environmental Science and Technology 33, 3506–3515.

Hughes, L.S., Allen, J.O., Bhave, P., Kleeman, M.J., Cass, G.R., Liu, D.Y., Fergenson, D.P., Morrical, B.D., Prather, K.A., 2000. Evolution of atmospheric particles along trajectories crossing the Los Angeles basin. Environmental Science and Technology 34, 3058–3068.

Hughes, L.S., Allen, J.O., Salmon, L.G., Mayo, P.R., Johnson, R.J., Cass, G.R., 2002. Evolution of nitrogen species air pollutants along trajectories crossing the Los Angeles area. Environmental Science and Technology 36, 3928–3935.

Jacobson, M.Z., 1999. Studying the effects of calcium and magnesium on size-distributed nitrate and ammonium with EQUISOLV II. Atmospheric Environment 33, 3635–3649.

John, W., Wall, S.M., Ondo, J.L., Winklmayr, W., 1990. Modes in the size distributions of atmospheric inorganic aerosol. Atmospheric Environment 24A, 2349–2359.

Johnston, M.V., 2000. Sampling and analysis of individual particles by aerosol mass spectrometry. Journal of Mass Spectrometry 35, 505–585.

Kane, D.B., Johnston, M.V., 2001. Enhancing the detection of sulfate particles for laser ablation aerosol mass spectrometry. Analytical Chemistry 73, 5365–5369.

Kane, D.B., Wang, J.J., Frost, K., Johnston, M.V., 2002. Detection of negative ions from individual ultrafine particles. Analytical Chemistry 74, 2092–2096.

Kawamura, K., Steinberg, S., Kaplan, I.R., 2000. Homologous series of C1–C10 monocarboxylic acids and C1–C6 carbonyls in Los Angeles air and motor vehicle exhaust. Atmospheric Environment 34, 4175–4191.

Kegler, S.R., Wilson, W.E., Marcus, A.H., 2001. PM1, intermodal (PM2.5-1) mass, and the soil component of PM2.5 in Phoenix, AZ, 1995–1996. Aerosol Science and Technology 35, 914–920.

Kerminen, V.-M., Teinila, K., Hillamo, R., Pakkanen, T., 1998. Substitution of chloride in sea-salt particles by inorganic and organic anions. Journal of Aerosol Science 29, 929–942.

Kim, B.M., Teffera, S., Zeldin, M.D., 2000a. Characterization of PM2.5 and PM10 in the South Coast Air Basin of southern California: Part 1—spatial variations. Journal of the Air and Waste Management Association 50, 2034–2044.

Kim, B.M., Teffera, S., Zeldin, M.D., 2000b. Characterization of PM2.5 and PM10 in the South Coast Air Basin of southern California: Part 2—Temporal variations. Journal of the Air and Waste Management Association 50, 2045–2059.

Kleeman, M.J., Cass, G.R., 2001. A 3D Eulerian source-oriented model for an externally mixed aerosol. Environmental Science and Technology 35, 4834–4848.

Kleeman, M.J., Cass, G.R., Eldering, A., 1997. Modeling the airborne particle complex as a source-oriented external mixture. Journal of Geophysical Research-Atmospheres 102, 21355–21372.

Kleeman, M.J., Schauer, J.J., Cass, G.R., 1999. Size and composition distribution of fine particulate matter emitted from wood burning, meat charbroiling, and cigarettes. Environmental Science and Technology 33, 3516–3523.

Laden, F., Neas, L.M., Dockery, D.W., Schwartz, J., 2000. Associations of fine particulate matter from different sources with daily mortality in six US Cities. Environmental Health Perspectives 108, 941–955.

Lawson, D.R., 1990. The southern California air quality study. Journal of the Air and Waste Management Association 40, 156–165.

Lee, S.-H., Murphy, D.M., Thomson, D.S., Middlebrook, A.M., 2002. Chemical components of single particles measured with particle analysis by laser mass spectrometry (PALMS) during the Atlanta Supersite project: focus on organic/sulfate, lead, soot, and mineral particles. Journal of Geophysical Research-Atmospheres 107, AAC 1–13.

Liu, D.-Y., Prather, K.A., Hering, S.V., 2000. Variations in the size and chemical composition of nitrate-containing particles in Riverside, CA. Aerosol Science and Technology 33, 71–86.

Liu, D.-Y., Wenzel, R.J., Prather, K.A., 2003. Aerosol time-of-flight mass spectrometry during the Atlanta Supersite experiment. Part 1: Measurements. Journal of Geophysical Research-Atmospheres 108, SOS 14-1:14-16.

Lurmann, F.W., Wexler, A.S., Pandis, S.N., Musarra, S., Kumar, N., Seinfeld, J.H., 1997. Modelling urban and regional aerosols. 2. Application to California's south coast air basin. Atmospheric Environment 31, 2695–2715.

Lyyranen, J., Jokiniemi, J., Kauppinem, E.I., Joutsensaari, J., 1999. Aerosol characterisation in medium speed diesel engines operating with heavy fuel oils. Journal of Aerosol Science 30, 771–784.

Mallina, R.V., Wexler, A.S., Rhoads, K.P., Johnston, M.V., 2000. High speed particle beam generation: a dynamic focusing mechanism for selecting ultrafine particles. Aerosol Science and Technology 33, 87–104.

McMurry, P.H., 2000. A review of atmospheric aerosol measurements. Atmospheric Environment 34, 1959–1999.

Meng, Z.Y., Seinfeld, J.H., 1996. Time scales to achieve atmospheric gas-aerosol equilibrium for volatile species. Atmospheric Environment 30, 2889–2900.

Middlebrook, A.M., Murphy, D.M., Lee, S., Thomson, D.S., Prather, K., Wenzel, R., Liu, D.Y., Phares, D., Rhoads, K.P., Wexler, A.S., Johnston, M.V., Jimenez, J., Jayne, J.T., Worsnop, D.R., Yourshaw, I., Seinfeld, J.H., Flagan, R.C., Hering, S.V., Weber, R.J., Jongejan, P., Slanina, J., Dasgupta, P., 2003. A comparison of particle mass spectrometers during the 1999 Atlanta Supersite experiment. Journal of Geophysical Research-Atmospheres 108, SOS 12-1:12-13.

Morawska, L., Zhang, J.F., 2002. Combustion sources of particles. 1. Health relevance and source signatures. Chemosphere 49, 1045–1058.

Murphy, D.M., Thomson, D.S., 2000. Halogen ions and no + in the mass spectra of aerosols in the upper troposphere and lower stratosphere. Geophysical Research Letters 27, 3217–3220.

Murphy, D.M., Thomson, D.S., Mahoney, T.M.J., 1998. In situ measurements of organics, meteoritic material, mercury, and other elements in aerosols at 5 to 19 kilometers. Science 282, 1664–1669.

Neubauer, K.R., Johnston, M.V., Wexler, A.S., 1998. Humidity effects on the mass spectra of single aerosol particles. Atmospheric Environment 32, 2521–2529.

Noble, C.A., Prather, K.A., 1996. Real-time measurement of correlated size and composition profiles of individual atmospheric aerosol particles. Environmental Science and Technology 30, 2667–2680.

Pandis, S.N., Harley, R.A., Cass, G.R., Seinfeld, J.H., 1992. Secondary organic aerosol formation and transport. Atmospheric Environment 26A, 2269–2282.

Penner, J.E., Hegg, D., Leaitch, R., 2001. Unraveling the role of aerosols in climate change. Environmental Science and Technology 35, 332A–340A.

Phares, D.J., Rhoads, K.P., Wexler, A.S., Kane, D.B., Johnston, M.V., 2001. Application of the ART-2a algorithm to laser ablation aerosol mass spectrometry of particle standards. Analytical Chemistry 73, 2338–2344.

Pilinis, C., Seinfeld, J.H., Seigneur, C., 1987. Mathematical modeling of the dynamics of multicomponent atmospheric aerosols. Atmospheric Environment 21, 943–955.

Pitchford, M., Green, M., 1997. Analyses of sulfur aerosol size distributions for a forty-day period in summer, 1992 in Meadview, Arizona. Journal of the Air and Waste Management Association 47, 136–146.

Pope, C.A., 2000. Review: epidemiological basis for particulate air pollution health standards. Aerosol Science and Technology 32, 4–14.

Prather, K.A., Nordmeyer, T., Salt, K., 1994. Real-time characterization of individual aerosol particles using time-of-flight mass spectrometry. Analytical Chemistry 66, 1403–1407.

Raes, F., Van Dingenen, R., Vignati, E., Wilson, J., Putaud, J.-P., Seinfeld, J.H., Adams, P., 2000. Formation and cycling of aerosols in the global troposphere. Atmospheric Environment 34, 4215–4240.

Roth, B., Okada, K., 1998. On the modification of sea-salt particles in the coastal atmosphere. Atmospheric Environment 32, 1555–1569.

Russell, A.G., Cass, G.R., 1986. Verification of a mathematical model for aerosol nitrate and nitric acid formation, and its use for control measure evaluation. Atmospheric Environment 20, 2011–2025.

Russell, A.G., McCue, K.F., Cass, G.R., 1988. Mathematical modeling of the formation of nitrogen-containing air pollutants. 1. Evaluation of an Eulerian photochemical model. Environmental Science and Technology 22, 263–271.

Salma, I., Maso, M.D., Kulmala, M., Zaray, G., 2002. Modal characteristics of particulate matter in urban atmospheric aerosols. Microchemical Journal 73, 19–26.

Silva, P.J., Carlin, R.A., Prather, K.A., 2000. Single particle analysis of suspended soil dust from southern California. Atmospheric Environment 34, 1811–1820.

Singh, M., Jaques, P.A., Sioutas, C., 2002. Size distributions and diurnal characteristics of particle-bound metals in source and receptor sites of the Los Angeles basin. Atmospheric Environment 36, 1675–1689.

Solomon, P.A., Larson, S.M., Fall, T., Cass, G.R., 1988. Basinwide nitric acid and related species concentrations observed during the Claremont nitrogen species comparison study. Atmospheric Environment 22, 1587–1594.

Solomon, P.A., Fall, T., Salmon, L., Cass, G.R., Gray, H.A., Davidson, A., 1989. Chemical characteristics of PM10 aerosols collected in the Los Angeles area. Journal of the Air Pollution Control Association 39, 154–163.

Song, X.-H., Hopke, P.K., Fergenson, D.P., Prather, K.A., 1999. Classification of single particles analyzed by ATOFMS using an artificial neural network, ART-2a. Analytical Chemistry 71, 860–865.

Suarez, A.E., Ondov, J.M., 2002. Ambient aerosol concentrations of elements resolved by size and source: contributions of some cytokine-active metals from coal- and oil-fired power plants. Energy and Fuels 16, 562–568.

Suess, D.T., Prather, K.A., 1999. Mass spectrometry of aerosols. Chemical Reviews (Washington, DC) 99, 3007–3035.

Tan, P.V., Malpica, O., Evans, G.J., Owega, S., Fila, M.S., 2002. Chemically-assigned classification of aerosol mass spectra. Journal of the American Society for Mass Spectrometry 13, 826–838.

Thomas, S., Morawska, L., 2002. Size-selected particles in an urban atmosphere of Brisbane, Australia. Atmospheric Environment 36, 4277–4288.

Turpin, B.A., Huntzicker, J.J., 1995. Identification of secondary organic aerosol episodes and quantitation of primary and secondary organic aerosol concentrations during SCAQS. Atmospheric Environment 29, 3527–3544.

Vedal, S., 1997. Ambient particles and health: lines that divide. Journal of the Air and Waste Management Association 47, 551–581.

Wall, S.M., John, W., Ondo, J.L., 1988. Measurement of aerosol size distributions for nitrate and major ionic species. Atmospheric Environment 22, 1649–1656.

Watson, J.G., 2002. Visibility: science and regulation. Journal of the Air and Waste Management Association 52, 628–713.

Watson, J.G., Chow, J.C., Lowenthal, D.H., Pritchett, L.C., Frazier, C.A., 1994. Differences in the carbon composition of source profiles for diesel- and gasoline-powered vehicles. Atmospheric Environment 28, 2493–2505.

Wenzel, R.J., Liu, D.Y., Edgerton, E., Prather, K.A., 2003. Aerosol time-of-flight mass spectrometry during the Atlanta Supersite experiment: 2. Scaling procedures Journal of Geographical Research-Atmospheres 108, SOS 15-1:15-8.

Wexler, A.S., Seinfeld, J.H., 1992. Analysis of aerosol ammonium nitrate: departures from equilibrium during SCAQS. Atmospheric Environment 26A, 579–591.

Wilson, W.E., Chow, J.C., Claiborn, C., Wei, F.S., Engelbrecht, J., Watson, J.G., 2002. Monitoring of particulate matter outdoors. Chemosphere 49, 1009–1043.